

Effect of front TCO on the performance of rear-junction silicon heterojunction solar cells: Insights from simulations and experiments

Alexandros Cruz^a, Er-Chien Wang^a, Anna B. Morales Vilches^a, Daniel Meza^b, Sebastian Neubert^a, Bernd Szyszka^c, Rutger Schlatmann^a, Bernd Stannowski^a

^aHelmholtz-Zentrum Berlin, PVcomB, Schwarzschildstr. 3, 12489 Berlin, Germany

^bHelmholtz-Zentrum Berlin, Institute for Silicon Photovoltaics, Kekuléstraße 5, 12489 Berlin, Germany

^cTechnische Universität Berlin, Einsteinufer 25, 10587 Berlin, Germany

alexandros.cruz@helmholtz-berlin.de, er-chien.wang@helmholtz-berlin.de, ana.morales_vilches@helmholtz-berlin.de, daniel.meza@helmholtz-berlin.de, sebastian.neubert@helmholtz-berlin.de, bernd.szyszka@tu-berlin.de, rutger.schlatmann@helmholtz-berlin.de, bernd.stannowski@helmholtz-berlin.de

Corresponding Author: Alexandros Cruz^a; alexandros.cruz@helmholtz-berlin.de

Abstract — In this study we make a detailed comparison between indium tin oxide (ITO), aluminum-doped zinc oxide (ZnO:Al) and hydrogenated indium oxide (IO:H) when applied on the illuminated side of rear-junction silicon heterojunction (SHJ) solar cells. ITO being the state of the art material for this application, ZnO:Al being an attractive substitute due to its cost effectiveness and IO:H being a transparent conductive oxide (TCO) with high-mobility and excellent optical properties. Through numerical simulations, the optically optimal thicknesses for a double layer anti-reflective coating system, consisting of the respective TCO and amorphous silicon oxide (a-SiO₂) capping layers are defined. Through two-dimensional electrical simulations, we present a comparison between front-junction and rear-junction devices to show the behavior of series resistance (R_s) in dependence of the TCO sheet resistance (R_{sh}) and the device effective lifetime (τ_{eff}). The study indicates that there is a τ_{eff} dependent critical TCO R_{sh} value, above which, the rear-junction device will become advantageous over the front-junction design in terms of R_s . Solar cells with the respective layers are analyzed. We show that a thinner TCO optimized layer will result in a benefit in cell performance when implementing a double layer anti-reflective coating. We conclude that for a highest efficiency solar cell performance, a high mobility TCO, like IO:H, is required as the device simulations show. However, the rear-junction solar cell design permits the implementation of a lower conductive TCO in the example of the cost-effective ZnO:Al with comparable performance to the ITO, opening the possibility for substitution in mass production.

Keywords: Transparent conductive oxide, Silicon heterojunction, Rear-junction, Sheet resistance, Anti-reflective coating, Series resistance

1. Introduction

Silicon heterojunction (SHJ) solar cells have gained significant interest in the past years due to their high performance, with record efficiencies of 25.1% and 26.7% for two-side and all-back contacted cells, respectively [1][2][3]. The main driver for these achievements has been the excellent passivation of the crystalline silicon (c-Si) wafer by thin hydrogenated amorphous silicon (a-Si:H) contacts for electrons and holes leading to high open circuit voltages (V_{oc}). Unlike silicon solar cells with diffused (homo)junction for which the carriers are transported to the metal contacts within the wafer, the SHJ cell concept requires transparent conductive oxide (TCO) layers on top of the a-Si:H contacts for efficient lateral carrier transport towards the metal contacts. The development of TCO materials with high-mobility and low parasitic absorption facilitated short circuit current densities (J_{sc}) of over 40 mA/cm² with fill factors (FF) well above 80% [4].

In today's crystalline silicon solar cells the (homo)junction is usually placed at the front (illuminated) side of the wafer for various reasons, e.g. to support the collection of minority carriers with a shorter average path length to the illuminated side. For the SHJ, however, the design rules are different. This is due to the symmetric design of electron and hole contacts as well as the use of monocrystalline silicon wafers (usually n-type) with very high carrier lifetimes, hence long diffusion lengths. Placing the junction on the rear side allows the wafer to support the front side TCO to laterally transport the majority carriers and, in turn, relaxes the requirements on the conductivity of the front TCO. This was shown and discussed in depth by Bivour *et al.* [5]. Here we present a detailed comparison of different front-TCOs and its effect on the performance of SHJ solar cells both by simulations and in experimental cells. The investigated TCOs are indium tin oxide (ITO), aluminum-doped zinc oxide (ZnO:Al) and hydrogenated indium oxide (IO:H). ITO has good opto-electrical properties and long-term stability [6], which is the reason for its widespread use for optoelectronic applications and has become a standard material for SHJ solar cells. ZnO:Al is a natively

polycrystalline material with lower electronic quality than ITO when deposited at low temperatures (< 200°C) and as thin layer (<100 nm). The abundance of zinc in the earth's crust, however, makes it an attractive low-cost substitute for indium-based TCOs [7]. IO:H on the other hand is a TCO with carrier mobility over 100 cm²/Vs and low parasitic absorption [8]. In our study we investigated two cases: firstly, a TCO thickness of 75 nm, typical for best anti-reflection (AR) effect with solar irradiation (AM1.5g) on silicon [9] and secondly, thinner optimized TCO layers for reduced parasitic absorption. In both cases we added an a-SiO₂ layer as second AR layer on top to further reduce reflection losses [10]–[14]. For the analysis we carried out optical simulations with the Matlab-based one-dimensional program GenPro4 [15]. By adapting the TCO and the a-SiO₂ thicknesses, we optimized this layer system for highest photocurrent density of the SHJ device for each of the three investigated materials. Once the optimal thicknesses were known, electrical simulations were carried out with the two-dimensional program Quokka2 [16] to rate the total opto-electrical device performance, which is then compared to the performance of experimental cells. As a result we show, that the IO:H leads to highest efficiencies according to simulations. However, thanks to the rear-junction cell design the use of ZnO:Al as a front-TCO is possible without having a significant efficiency penalty.

2. Materials and Methods

2.1. TCO Deposition and Characterization

TCO layers with thicknesses of 105±10 nm measured with a Dektak profilometer were deposited on 1.1 mm thick Corning Eagle glass in an in-line DC magnetron sputtering system from Leybold Optics (A600V7). Such TCO layers have an approx. thickness of 75 nm when deposited on textured wafers as described in section 2.2. ITO layers were sputtered from a planar 97:3 In₂O₃:SnO₂ target, ZnO:Al from a rotatable 99:1 ZnO:Al₂O₃ target, and IO:H from a ceramic planar In₂O₃ target. ITO and ZnO:Al were deposited at an approximate substrate temperature of 150°C with oxygen flow ratios $r(\text{O}_2)=q(\text{O}_2)/q(\text{Ar}+\text{O}_2)$ of 2.4% and 0.48%, respectively. IO:H was deposited without intentional heating at an oxygen flow ratio of 2.0% and with an introduction of water vapor resulting in 1.7x10⁻⁶ mbar partial pressure. The depositions were carried out at a pressure of 2.6, 3.6 and 4.4 μbar for ITO, ZnO:Al and IO:H respectively. The system base pressure was of approx. 0.4 μbar in the sputtering chamber before any intentional gas inlet. The IO:H samples were post-deposition annealed in vacuum at 180°C for 1 h for crystallization.

Charge carrier mobility, μ_{Hall} , and concentration, N_c , were determined for TCO layers on glass by Hall measurements with an Ecopia HMS 3000 system applying the van der Pauw method at room temperature. The optical characterization of the TCOs was carried out with a Perkin Elmer Lambda 1050 spectrophotometer equipped with a 150 mm integrating sphere. Refractive indices n and extinction coefficients k of TCO samples deposited on glass and on flat silicon substrates were extracted from spectrophotometer and spectroscopic ellipsometry measurements by fitting to a Drude-Tauc-Lorentz model [17].

2.2. Solar Cells Preparation and Characterization

For solar cells preparation, n-type Czochralski (CZ) silicon wafers (c-Si) with 5 Ωcm resistivity were used. The as-cut wafers were wet-etched to remove the saw damage. Its surfaces were then chemically textured in KOH to obtain random pyramids with heights in the range of 2 – 4 μm with <111> oriented facets and resulting in 125-μm thick wafers. After RCA cleaning [18] finalized with a dip in a 1% diluted hydrofluoric acid solution, intrinsic and doped silicon layers were deposited by plasma enhanced chemical vapor deposition (PECVD) in an AKT1600 cluster tool from Applied Materials with a parallel electrode configuration operated at 13.56 MHz. An i/p a-Si:H stack was deposited on the rear side to form the hole contact (junction). At the front side an electron contact was formed by depositing an i-a-Si:H with an n-type nanocrystalline silicon (nc-Si:H) layer on top. Further details of the silicon thin-films used can be found elsewhere [19].

Monofacial solar cells were prepared by varying the front TCO layers and with a ZnO:Al/silver rear reflector. These layers were sputtered through aligned shadow masks on both sides of the wafer to define 4-cm² size cells and transfer length method (TLM) structures. Only the IO:H coated solar cells, underwent a thermal annealing process of 1 h at 185°C under vacuum in order to solid-phase crystallize the TCO. A silver grid with 1670 μm pitch and 50 μm finger thickness resulting in ~3% total shading was screen printed on the front TCO and subsequently cured at 210°C for 15 minutes on a hot-plate under atmospheric conditions. Finally, a PECVD a-SiO₂ layer was deposited on top of the finished devices as second anti-reflective coating. The process was carried out at gas flows of 4.5, 900 and 500 sccm for SiH₄, H₂, N₂O, respectively, at 185 °C and at 30 W.

The solar cells were characterized using current voltage ($J-V$) measurements in the dark and under an AM1.5G spectrum at standard test conditions in a Wacom WXS-155S-L2 dual source class AAA+ sun simulator. Resistance measurements on the TLM structures to calculate TCO-silver contact resistivity and TCO sheet resistance (R_{sh}) on devices were carried out. To derive the front TCO R_{sh} from a rear-junction device from TLM structures we used a parallel resistance model as proposed by Bivour et al. [5]. According to $R_{sh\ TCO} = 1 / (1 / R_{sh\ TLM} - 1 / R_{sh\ Wafer})$ with $R_{sh\ TCO}$ being the TCO sheet resistance, $R_{sh\ TLM}$ the sheet resistance measured via TLM structures and $R_{sh\ Wafer}$ the sheet resistance of the wafer. The wafer sheet resistance was kept constant at 400 Ω calculated from the nominal resistivity of the wafers of 5 Ωcm divided by its thickness nominally of 125 μm.

Series Resistance (R_s) values of the solar cells were determined from the dark to light $J-V$ curve comparison after Pysch *et al.* [20].

3. Results and Discussion

3.1. TCO Layer Properties

3.1.1. Electrical Properties

Sputtered ITO exhibits $\mu_{\text{Hall}} > 30 \text{ cm}^2/\text{Vs}$ in a broad range of carrier concentrations from 1 to $4 \times 10^{20} \text{ cm}^{-3}$ even for thin layers $< 100 \text{ nm}$ [21]. ZnO:Al layers, in contrast, reach these values only when deposited as several 100 nm thick layers typically at temperatures well above 200°C so that large crystal grains can be formed during growth. With the restrictions given by the SHJ solar cell processing, namely $< 100 \text{ nm}$ TCO thickness and temperatures $< 200^\circ\text{C}$, the ZnO:Al properties worsen, i.e. the 100-nm thick ZnO:Al layers here reach mobilities of only $10 - 20 \text{ cm}^2/\text{Vs}$, limited by the small-grained polycrystalline growth [22]. In comparison, IO:H is a high-mobility TCO reaching $\mu_{\text{Hall}} > 100 \text{ cm}^2/\text{Vs}$ even for very thin layers processed below 200°C . Koida *et al.* demonstrated that these remarkable values are due to solid-phase crystallization upon post-deposition annealing leading to lateral grain sizes up to 400 nm with relaxed grain boundaries that are formed from the as-deposited amorphous material. During sputtering the crystal growth is suppressed by adding water (H_2O) vapor to the argon process gas [23]. We optimized the deposition parameters for $105 \pm 10 \text{ nm}$ thick TCO layers on glass towards lowest carrier concentration possible in order to minimize the free-carrier absorption (FCA), yet still showing high mobility values. As we can see in Figure 1 the carrier concentration for the three TCOs investigated, remains within a narrow range of $2 \pm 0.5 \times 10^{20} \text{ cm}^{-3}$, hence the difference in conductivity between them is dominated by their μ_{Hall} . For the TCOs implemented in devices the values for μ_{Hall} are around 35 , 20 , and $100 \text{ cm}^2/\text{Vs}$, for ITO, ZnO:Al, and IO:H, respectively, with corresponding R_{sh} of $70 \pm 10 \Omega$, $190 \pm 20 \Omega$, and $30 \pm 10 \Omega$. For simulations we calculated the sheet resistance from the equation $R_{\text{sh}} = \rho/t$ where ρ is the specific resistivity and t is the thickness of the material. Depending on the type of TCO the value for ρ might vary with t as well as when being deposited on textured silicon wafers instead of glass. These effects, however, were neglected in our calculations for simplification. The contribution of the resistive losses related to the electrical properties of the TCOs and when varying the thickness of the respective materials on devices, was calculated with the Quokka2 program and is discussed in the electrical simulations section 3.2.2.

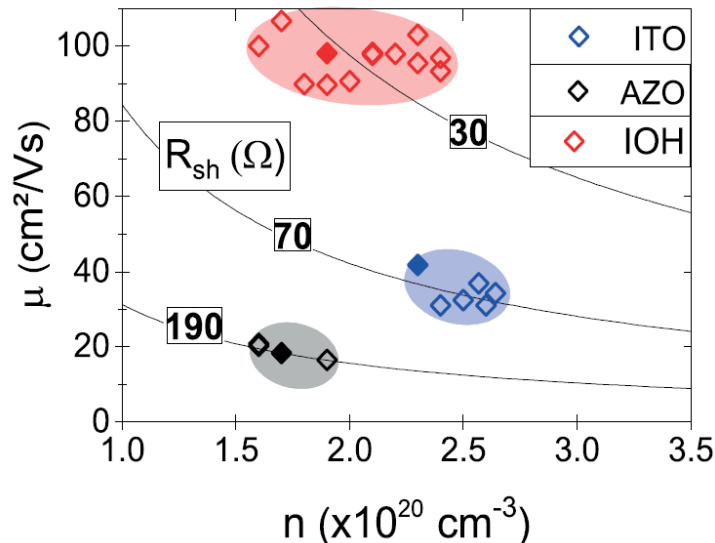


Figure 1. Mobility vs carrier concentration of $105 \pm 10 \text{ nm}$ thick ITO, ZnO:Al and IO:H layers on glass. The colored ellipses highlight the range of TCO properties applied on SHJ experimental solar cells. The filled symbols correspond to layers optically analyzed. The sheet resistance is calculated and plotted for 105 nm TCO thickness.

3.1.2. Optical Properties

To evaluate the optical properties of the different TCOs on glass, total reflection R and total transmission T spectra were measured for wavelengths from 300 to 1200 nm. Figure 2 shows absorption spectra calculated as $A = I - T - R$. Additionally, the simulated SHJ solar cell generated current density of our standard cell stack with an assumed TCO extinction coefficient $k = 0$ is shown to highlight the range where the parasitic absorption of the TCOs is most relevant. In the near infrared range > 700 nm the ITO has higher absorption than the ZnO:Al and the IO:H mostly due to its higher carrier concentration resulting in free carrier absorption (FCA). This trend continues towards shorter wavelengths where the IO:H and the ZnO:Al still have a lower sub-bandgap absorption than the ITO. This sub-bandgap absorption is usually ascribed to defects, such as point defects, dislocations, or grain boundaries [24]. Here, the IO:H shows noticeable lower absorption than both other materials by combining a high optical bandgap, and a low sub-bandgap absorption. Furthermore the high mobility of the IO:H helps suppress the FCA [25]. At a value around 400 nm the ZnO:Al suffers from the onset of the fundamental absorption due to its smaller optical bandgap of around 3.6 eV in comparison to 4.0 eV for the indium-based TCOs. In total, this makes IO:H the most transparent material in the relevant range followed by the ZnO:Al. For thinner layers, as we see in the example of the IO:H with 55 ± 5 nm thickness as the dashed line in Figure 2, the absorption can be further reduced.

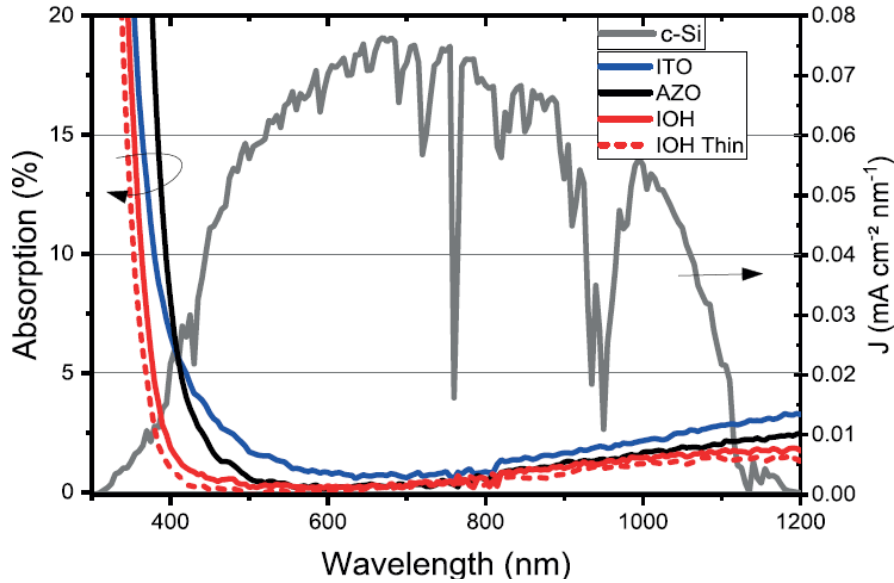


Figure 2. Optical absorption spectra of selected 105 ± 10 nm ITO, ZnO:Al and IO:H layers on glass and generated current density per wavelength of a standard SHJ solar cell from GenPro4 simulations. The dashed line is for a thinner IO:H 55 ± 5 nm layer.

3.2. Device Simulations

3.2.1. Optical Simulations

To quantify the optical performance of the TCO materials when integrated in SHJ cell in terms of J_{sc} , simulations with the Matlab-based program GenPro4 [15] were carried out for the complete cell stack. For this purpose, the TCO thickness as well as the one of the $a\text{-SiO}_2$ capping layer were varied. GenPro4 uses a ray-tracing model and the net-radiation method to calculate the interface reflectance, interface transmittance and layer absorption for each component in the material stack [15].

From the simulations the optimal double layer anti-reflective coating thicknesses for the solar cells were calculated to be considered for the electrical calculations in section 3.2.2. and to define the layer thicknesses for the experimental solar cells. It is known that the electrical properties of the TCOs change when deposited on hydrogenated silicon thin-films and when hydrogenated layers are then afterwards deposited on top of them [12][26]. This effect is expected to have an impact on the optical properties of the materials as well. To our knowledge, no detailed study on the variation of the optical properties of the TCO due to adjacent hydrogenated layers for SHJ solar cells has been published and this effect would be worth of detailed investigation and comparison. For this paper, we define the trends for optimal thicknesses of the layers considering the optical properties extracted from layers on glass and for fixed optical constants throughout the thickness variations.

In Figure 3 we display the current density loss due to parasitic absorption in the TCO $J_{Abs\ TCO}$ in dependence of the material thickness for each TCO for a solar cell stack without $a\text{-SiO}_2$ second anti-reflective layer.

Higher current gain will be obtained for the higher absorptive TCO layers when lowering the material thickness. Taking a 40 nm TCO thickness for comparison to the 75 nm standard thickness reference point, the IO:H gain is of 0.2 mA/cm² whereas the ITO and AZO thinning results in 0.4 and 0.7 mA/cm² gain, respectively.

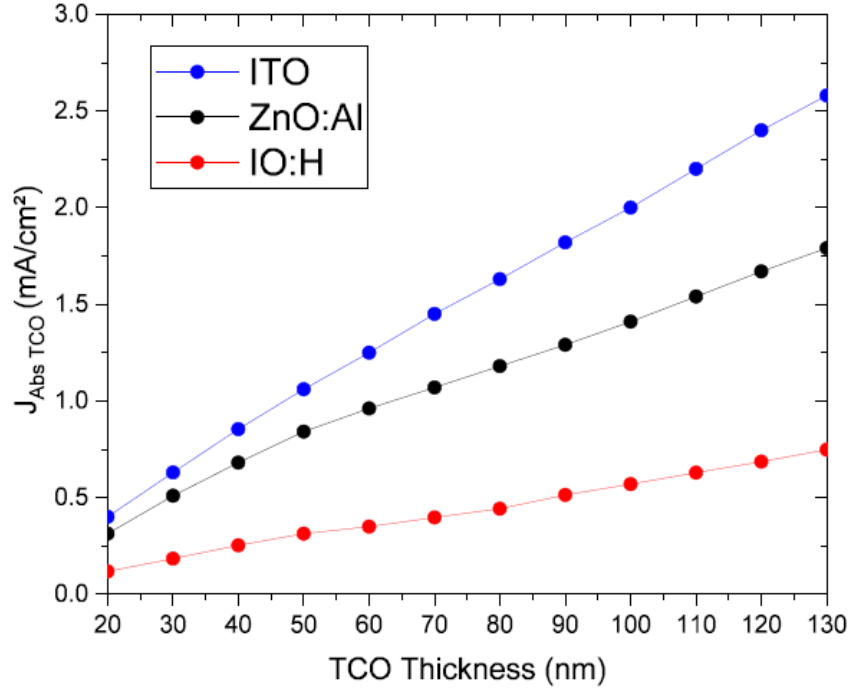


Figure 3. Current density loss due to parasitic absorption in the TCO $J_{Abs\ TCO}$ in dependence of the material thickness for a solar cell stack without a-SiO₂ second anti-reflective layer.

In the top row of Figure 4 we see the device reflection loss $J_{Reflection}$ color-maps for the different TCOs. The double layer anti-reflection coating optimum is positioned at slight lower TCO thicknesses than 75 nm. Further reducing the TCO thickness from these points will present a trade-off between the TCO absorption decrease and the device reflection losses. A device with a more absorptive TCO will generate its maximum current density $J_{Generated}$ with thinner TCO layers further away from its anti-reflective optimum. We confirm this in the lower row of Figure 4 where $J_{Generated}$ values for the devices at standard 75 nm thickness and at the double layer anti-reflective optimum are noted as calculated from simulations for our solar cell material stack. The optimum thicknesses of the TCO layers are extracted being of 40, 40 and 55 nm for ITO, ZnO:Al and IO:H, respectively. A decreased TCO thickness will result in a higher R_{sh} and can increase the device's series resistance R_s . Therefore, in the next section we quantify the R_s losses in the cell by means of electrical device simulations.

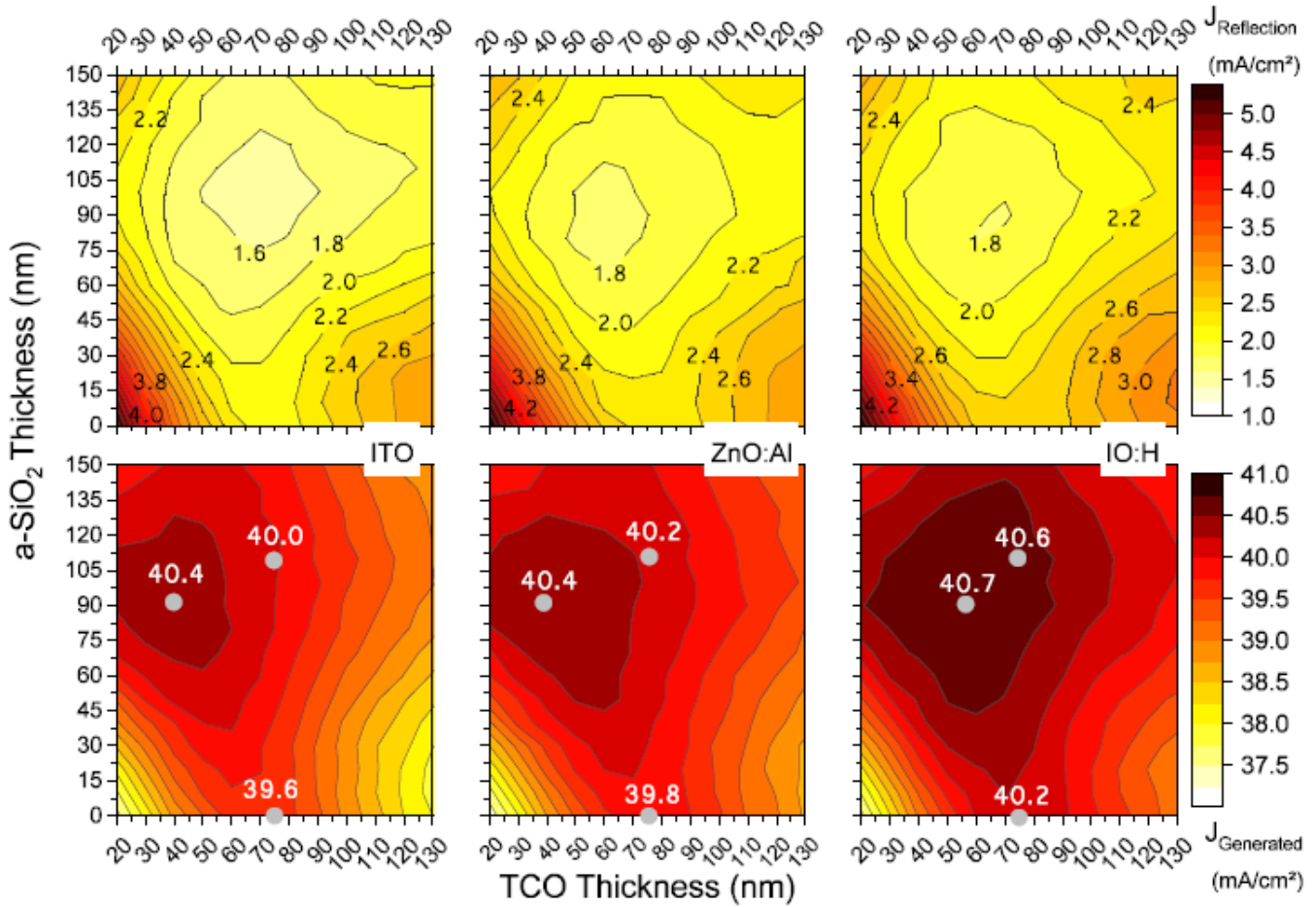


Figure 4. Top row: Colormaps of current density loss due to device reflection $J_{Reflection}$. Bottom row: Colormaps of current density generated $J_{Generated}$ in the device. For all graphs the TCO (ITO, ZnO:Al and IO:H) and the a-SiO₂ second ARC thickness on simulated silicon heterojunction solar cells are varied. Generated current in the silicon absorber $J_{Generated}$ values for 75 nm and optimal TCO thickness with and without a-SiO₂ optimal layers are noted.

3.2.2. Electrical Simulations

To simulate the electrical solar cell parameters, in particular to quantify the resistive transport losses in the wafer and in the different TCOs, Quokka2 was used, which facilitates simulations in two dimensions [16]. The geometry and material properties of our standard solar cell with 1670 μm grid-finger pitch (= 12 fingers) as described in the experimental methods section 2.2. was used. For the n-type silicon wafer the Klaassen [27] model was applied to describe electrons and holes mobility. Auger recombination was modelled following Richter's approach [28]. The radiative recombination coefficient was set to $4.73 \times 10^{-15} \text{ cm}^3$ according to Trupke *et al.* [29]. The bulk lifetime was varied from 500 to 9000 μs . For the rear ZnO:Al contacting layer a $R_{sh} = 200 \Omega$ was used. A dark saturation current density $J_0 = 5.5 \text{ fA/cm}^2$ and recombination current density of $J_{02} = 2.0 \text{ nA/cm}^2$ were determined from the two-diode model fit of our standard solar cell J - V curve and were introduced and assumed equally distributed for the rear and front side of the device. The R_{sh} of the front TCO was varied linearly with the TCO thicknesses. A geometry independent contact resistivity $\rho_c = 3 \text{ m}\Omega\text{cm}^2$ of the metal-TCO interface was determined by the TLM measurements [30] and introduced to the simulation. The current generation was assumed to occur at the surface of the device, with a steady value at 40.5 mA/cm² for an AM1.5 solar spectrum. A lumped external R_s of 0.4 Ωcm^2 was added to account for all remaining R_s contributions, i.e. the metal contact transport and the contact resistances at the remaining device interfaces. To calculate this value

we measured line resistivity of the screen-printed silver and measured the geometry of the grid fingers with a confocal microscope. For the TCO-Si contact resistivity, the R_s contribution was calculated by comparing the sum of all known contributions to the experimental value calculated from the light to dark J - V curves comparison.

Figure 5 shows the R_s calculated from the resistive power loss at maximum power point, as a function of the front TCO's R_{sh} and for two different effective carrier lifetimes τ_{eff} of the solar cells. One “low” at 400 μ s and one in the range of the ones calculated for our experimental devices, which lies at 1750 μ s and is hereafter referred to as “nominal”.

The average minority excess carrier density at operating point was calculated to be of $0.55 \pm 0.05 \times 10^{15} \text{ cm}^{-3}$ and $2.1 \pm 0.1 \times 10^{15} \text{ cm}^{-3}$ for the low and nominal τ_{eff} defined, respectively.

In Figure 5 at a 0 Ω R_{sh} TCO value the R_s consists exclusively of the external lumped R_s value of 0.4 Ωcm^2 plus the R_s accounting for the vertical charge carrier transport, since the lateral transport to the metal-grid will be carried out by the ideally conductive TCO without losses. We see from the simulations that the clearly higher R_s increase for the rear-junction in comparison to the front-junction device when τ_{eff} is decreased, is mainly dominated by the less conductive holes transport to the rear selective contact. For the front-junction device for which the electrons are the ones travelling to the rear contact, the τ_{eff} decrease will barely increase the R_s at this point.

When increasing the TCO R_{sh} , lateral transport losses will arise. We can see a clearly higher R_s increment with increasing R_{sh} for the front-junction device since the TCO is partially electrically separated from the wafer by the pn depletion region for this case. Still, some of the lateral transport will take part in the wafer for the front-junction device as the TCO R_{sh} increases and current-crowding at the TCO-Si interface forces the lateral charge carrier flow within the wafer. For the rear-junction device, the R_s increase due to the lateral transport is less pronounced, since the TCO and the wafer are electrically coupled as discussed by Bivour et al. [5].

Considering the solar cell type and the behavior of the R_s in dependence of the TCO R_{sh} for the nominal τ_{eff} , we see that for higher resistive TCOs the rear-junction design is clearly advantageous. Below $R_{sh} \approx 100 \Omega$, however, the front-junction device shows lower R_s . This is even more significant for the low τ_{eff} where the front- outperforms the rear-junction design in terms of R_s for TCOs of up to $R_{sh} = 300 \Omega$. This behavior highlights the importance of considering the effect of the TCO R_{sh} in combination with the τ_{eff} of the device when deciding on the design between a front-junction and a rear-junction device.

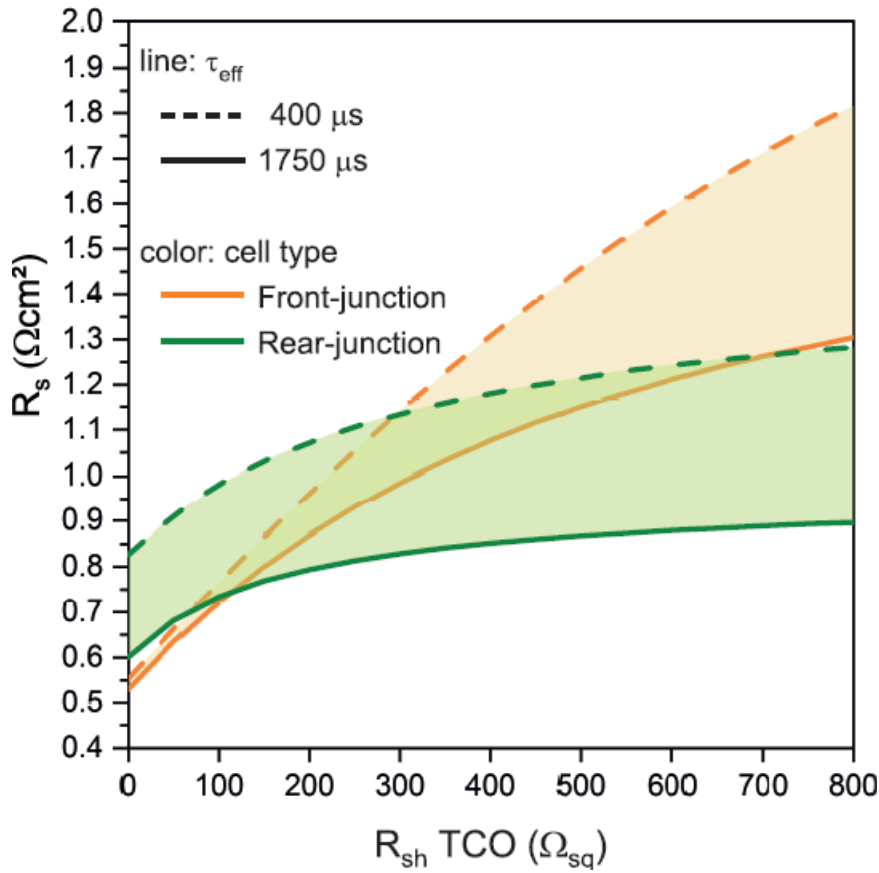


Figure 5. Simulated R_s dependence on front-TCO R_{sh} for rear-junction (green lines) and front-junction (orange lines) devices with 400 μs (dashed lines) and 1750 μs (solid lines) τ_{eff} lifetime.

3.2.3. Simulated Solar Cells Parameters

Based on the simulated values for J_{sc} , reduced by 3 % ($\sim 1.2 \text{ mA/cm}^2$) due to the grid shading, and along with R_s obtained from the electrical simulations we can calculate the cell parameters. The open circuit voltage V_{oc} shows values from 729 to 730 mV slightly varying with the TCO's R_{sh} . Table 1 summarizes the simulated values for R_s , FF and the efficiency η for the “standard” 75 nm thick TCOs and for the thinner TCOs both with a-SiO₂ capping. When reducing the TCO thicknesses an R_s increase and FF decrease results, however the device η stays the same or even increases due to the optical performance benefit. We also see that the ZnO:Al front-contacted rear-junction device shows a very similar η of 22.7% in comparison to its ITO counterpart with 22.8%. In contrast, for a front-junction solar cell design the η of a ZnO:Al device considerably drops to 22.1%. The IO:H will result in the best efficiency being around 23% as compared to the other two TCO materials independently of the device configuration due to its higher conductivity.

Considering the grid-finger pitch, that was originally optimized for the cells with ITO, the ZnO:Al will slightly improve its η when narrowing the pitch to 1430 μm and, oppositely, the IO:H cells by increasing it to 1800 μm . Nonetheless, we found that this effect, has a small impact on the device efficiency of only $\pm 0.1 \%$ (abs), as we simulated the full effect of varying finger pitches at a constant finger width for all TCOs (not shown).

Table 1. Calculated R_{sh} from single layers on glass as well as simulated R_s , FF and η for standard and optimized front-contact TCO thicknesses. At optimized TCO thickness R_s , FF and η are shown for a front-emitter cell design simulation for comparison.

TCO	Standard TCO thickness rear-junction					Optimized TCO thickness rear-junction					Optimized TCO thickness front-junction		
	t (nm)	R_{sh} (Ω)	R_s (Ωcm^2)	FF (%)	η (%)	t (nm)	R_{sh} (Ω)	R_s (Ωcm^2)	FF (%)	η (%)	FF (%)	R_s (Ωcm^2)	η (%)
ITO	75	100	0.74	79.8	22.6	40	190	0.80	79.5	22.8	78.9	0.86	22.5
ZnO:Al	75	260	0.82	79.4	22.6	40	500	0.88	79.1	22.7	77.2	1.16	22.1
IO:H	75	60	0.70	80.1	23.1	55	80	0.72	80.0	23.1	79.8	0.69	22.9

3.3. Experimental Solar Cell Results

We prepared SHJ cells following the optimized and simulated designs as discussed above, namely, for all three TCOs the standard and the optimized thin version, both with a-SiO₂ capping. Figure 6 shows the J - V parameters of these cells. Generally, we observe that the trends in $J_{Generated}$ resemble the simulated ones. The IO:H clearly outperforms the other two TCOs in terms of current density and the cells with optimized TCO thicknesses generally perform better than the “standard” ones, while the largest benefit is found for the ITO, as expected. For V_{oc} and pFF , however, we observe effects that were not expected and were not considered in the Quokka2 simulations. Firstly, V_{oc} and pFF are mostly increased for the “optimized” TCO stack as compared to the “standard” one. Secondly, the cells with IO:H suffer $\sim 15 \text{ mV}$ V_{oc} loss and 2% (abs.) pFF loss as compared to the cells with ITO or ZnO:Al. The first observation might be explained by two effects: (1) the thinner TCO sputtering could result in less sputter damage, or (2) the deposition of the a-SiO₂ layer by PECVD leads to a curing effect due to the reactive hydrogen that is present during PECVD. The hydrogen might penetrate the TCO layer, subsequently, passivating defects at the Si surface. With a thinner TCO this passivation might be more effective due to the shorter penetration path, leading to improved V_{oc} and pFF . The second effect most likely can be ascribed to the IO:H processing, since the samples are thermally annealed in vacuum for one hour after TCO sputtering. Results of lifetime measurements (not shown) of c-Si/i-a-Si:H/p-a-Si:H (i/p) symmetric samples highlight that the thermal budget for this annealing process is excessive for the device, thereby, diminishing the passivation of the

c-Si wafer. There is a trade-off between the optimal crystallization of the IO:H and the passivation properties of the i/p layers after thermal processes. Optimizing this process step and avoiding the V_{oc} and pFF degradation should lead to the expected best cell efficiency $>23\%$ for IO:H. The main parameters that can be varied for this purpose are the annealing temperature, time and atmosphere (air, vacuum). We also can discard a strong difference in sputtering damage for the different devices. All devices became the same ZnO:Al/silver back contact at the i/p contact side and for the i/n passivating layers we have seen that the iFF and iV_{oc} are fully recovered after the respective annealing processes for all TCOs.

In order to test the initial assumption on the benefit of using a rear-junction configuration, as was shown in Figure 5 with the relation between the simulated cell's R_s and the TCO's R_{sh} , we plot experimental values of R_s vs. R_{sh} together with the simulated curves, shown in Figure 7. We found that after a-SiO₂ deposition the R_{sh} , as deduced from TLM measurements through the method described in section 2.2., is reduced by 20 to 45% for all three TCOs. For this reason, we see a discrepancy between the calculated values from the layers on glass described in section 3.1.1. when compared to those ones deduced from TLM structures on the wafer. Ritzau *et al.* [26] reported a similar effect. They observed a lowering of R_{sh} for ITO annealed on thin-film a-Si:H layers. Similar to that, Herasimneka *et al.* [12] noticed an R_{sh} reduction when depositing a-SiO_x:H on top of ITO layers as second ARC. As was also discussed above, hydrogen radicals, present during deposition of a-SiO₂ by PECVD, might diffuse through and into the TCO improving its electrical properties, e.g. due to grain boundary passivation.

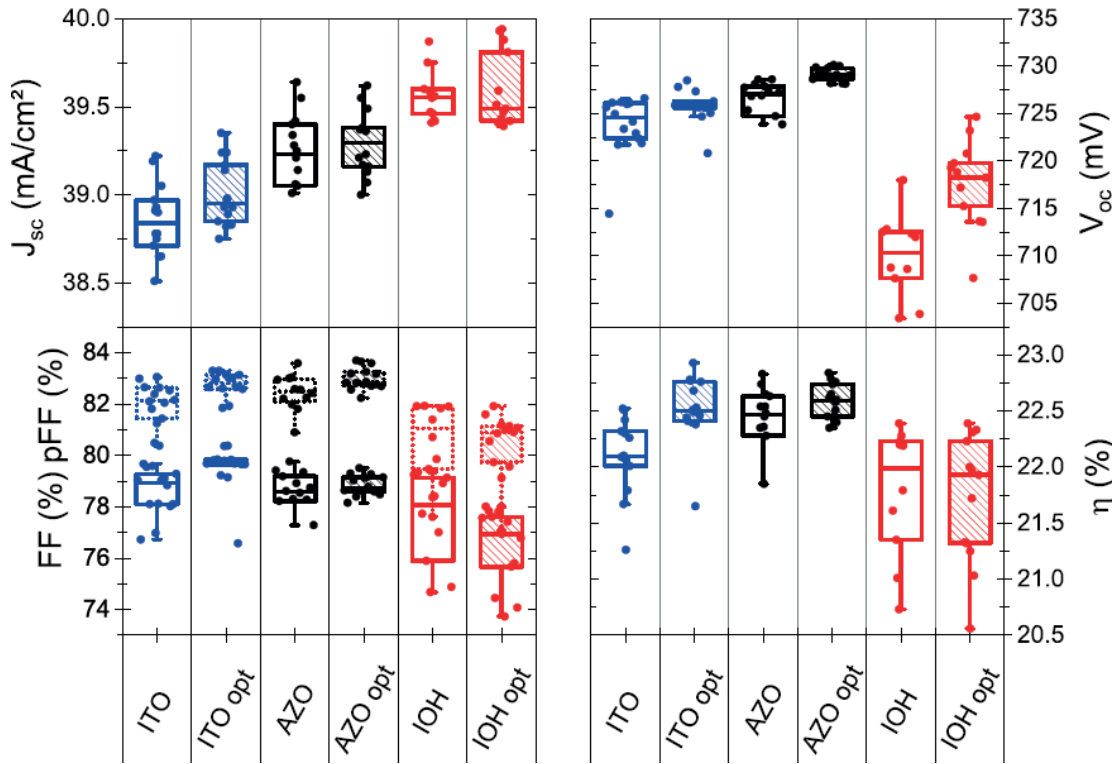


Figure 6. Current-voltage parameters of experimental cells that were prepared with a standard 75 nm TCO thickness and at their optimized thickness, both with a-SiO₂ capping (compare Figure 4). The pseudo fill-factor is plotted on the fill factor graph with dotted borders. The boxplots are shown with median values indicated.

In Figure 6 we see that even when using ZnO:Al with an R_{sh} as high as 250 Ω the cell's R_s is increased by only 0.2 Ωcm^2 as compared to the ITO reference. Also shown in the graph is the simulated trend for a front junction solar cell and the R_s value for the sample with highest R_{sh} with the thin ZnO:Al before a-SiO₂ capping. We see that in this R_{sh} range the experimental R_s value is higher than simulated for the rear-junction trend but clearly lower than expected for front-junction cells. This might be an indication of an overestimation of the lateral transport support by the wafer in this range. Moreover, there is uncertainty in the resistance contribution from the TCO/n-layer contact, which was included in the lumped R_s simulation value being the same for all samples. Nonetheless, we can confirm that the R_s of the cell with ZnO:Al remains in a competitive level when comparing to the ITO cell. Concerning the impact of the a-SiO_x layer on device stability under hot and humid atmosphere, Adachi *et al.* investigated the effects of a-SiO_x capping on SHJ solar cells as a barrier on top of ITO transparent electrodes and concluded that

this layer improves the damp-heat (DH) stability of encapsulated cells [31]. In a recent study we showed there is also a benefit for the stability of ZnO:Al contacted full-size encapsulated SHJ cells having same good stability as ITO references [32].

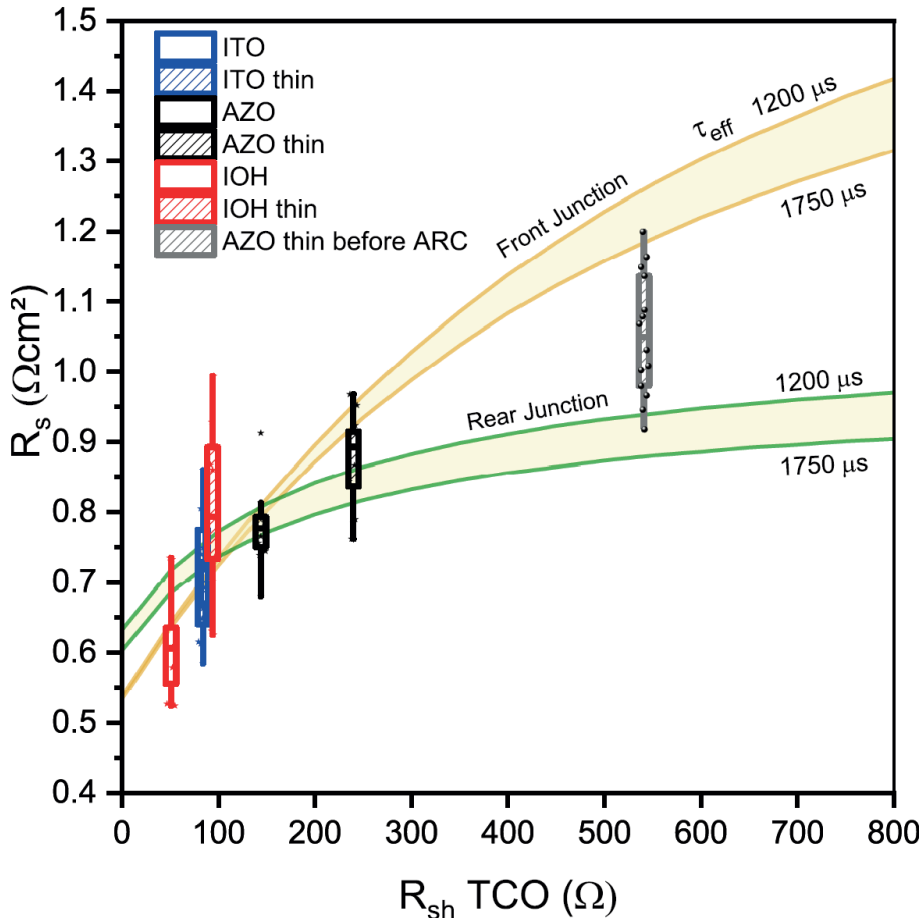


Figure 7. R_s values of experimental solar cells calculated from the dark to light $J-V$ curves comparison as a function of TCO R_{sh} extracted from TLM structures of the same samples. The simulated R_s for a τ_{eff} ranging from 1200 to 1750 μs for rear- and front-junction SHJ cells are added as a guideline (compare to Figure 5). The boxplots are shown with median values indicated.

4. Conclusions

In summary, we demonstrated by optical and electrical simulations as well as with experimental results the effect of different front TCOs on the performance of rear-junction SHJ solar cells. High-mobility TCOs, such as IO:H, are expected to outperform other TCOs under investigation, i.e. ITO and ZnO:Al, with a predicted efficiency benefit of 0.4% (abs.). In our experimental cell results, however, degradation of V_{oc} and pFF overcompensates the optical benefit. We expect to solve this by reducing the thermal budget during IO:H annealing. Experimental devices confirm that optimized thinner TCO layers will result in an

efficiency enhancement or, in the worst case, allow for the same performance while offering the advantage of cost reduction by TCO material saving. We showed the beneficial optical effect of a PECVD a-SiO₂ capping layer after TCO sputtering, as also proposed by other groups. Moreover, we found strong indications that this layer can even improve electrical cell properties, i.e. V_{oc} and pFF , in particular for thin TCOs, which we explain by hydrogen passivation of the silicon surface during the PECVD deposition.

The electrical simulations propose that a lesser conductive TCO in the example of ZnO:Al can be implemented in a rear-junction device without compromising the solar cell's R_s . Experimental results confirm, that the relatively resistive but very transparent ZnO:Al is an attractive alternative to ITO, yielding very similar efficiencies when implemented in rear-junction SHJ solar cells. These results pave the way for the application of the abundant and cost-effective ZnO:Al substituting indium-based TCOs in SHJ solar cell mass production.

Acknowledgement

We would like to thank the co-workers at HZB for their support. Katja Mayer-Stillrich and Manuel Hartig for sputtering depositions. Mathias Zelt and Tobias Henschel for support with PECVD. Holger Rhein for screen-printing processing. Darja Erfurt and Stefan Körner for fruitful discussions. Dr. Florian Ruske for support with ellipsometry measurements and optical modelling. This work was partially supported by the German Ministry of Economic Affairs and Energy (BMWi) in the framework of the HERA project (reference #03258251). Alexandros Cruz gratefully acknowledges the scholarship support from the Mexican National Council for Science and Technology (CONACYT).

Figure 1. Mobility vs carrier concentration of 105±10 nm thick ITO, ZnO:Al and IO:H layers on glass. The colored ellipses highlight the range of TCO properties applied on SHJ experimental solar cells. The filled symbols correspond to layers optically analyzed. The sheet resistance is calculated and plotted for 105 nm TCO thickness.

Figure 2. Optical absorption spectra of selected 105±10 nm ITO, ZnO:Al and IO:H layers on glass and generated current density per wavelength of a standard SHJ solar cell from GenPro4 simulations. The dashed line is for a thinner IO:H 55±5 nm layer.

Figure 3. Current gain or loss ΔJ in dependence of TCO thickness. The values are referenced to the current absorbed by each TCO at their standard thickness of 75 nm. Current gain values are noted for 40 nm TCO thickness.

Figure 4. Top row: Colormaps of current density loss due to device reflection $J_{Reflection}$. Bottom row: Colormaps of current density generated $J_{Generated}$ in the device. For all graphs the TCO (ITO, ZnO:Al and IO:H) and the a-SiO₂ second ARC thickness on simulated silicon heterojunction solar cells are varied. Generated current in the silicon absorber $J_{Generated}$ values for 75 nm and optimal TCO thickness with and without a-SiO₂ optimal layers are noted.

Figure 5. Simulated R_s dependence on front-TCO R_{sh} for rear-junction (green lines) and front-junction (orange lines) devices with 400 μs (dashed lines) and 1750 μs (solid lines) τ_{eff} lifetime.

Figure 6. Current-voltage parameters of experimental cells that were prepared with a standard 75 nm TCO thickness and at their optimized thickness, both with a-SiO₂ capping (compare Figure 4). The pseudo fill-factor is plotted on the fill factor graph as dotted lines. The boxplots are shown with median values indicated.

Figure 7. R_s values of experimental solar cells calculated from the dark to light $J-V$ curves comparison as a function of TCO R_{sh} extracted from TLM structures of the same samples. The simulated R_s for a τ_{eff} ranging from 1200 to 1750 μs for rear- and front-junction SHJ cells are added as a guideline (compare to Figure 5). The boxplots are shown with median values indicated.

REFERENCES

- [1] K. Yoshikawa *et al.*, "Silicon heterojunction solar cell with interdigitated back contacts for a photoconversion efficiency over 26%," *Nat. Energy*, vol. 2, no. 5, p. 17032, May 2017.

- [2] D. Adachi, J. L. Hernández, and K. Yamamoto, "Impact of carrier recombination on fill factor for large area heterojunction crystalline silicon solar cell with 25.1% efficiency," *Appl. Phys. Lett.*, vol. 107, no. 23, p. 233506, Dec. 2015.
- [3] M. A. Green *et al.*, "Solar cell efficiency tables (version 50)," *Prog. Photovolt. Res. Appl.*, vol. 25, no. 7, pp. 668–676, Jul. 2017.
- [4] J. Haschke, O. Dupré, M. Boccard, and C. Ballif, "Silicon heterojunction solar cells: Recent technological development and practical aspects - from lab to industry," *Sol. Energy Mater. Sol. Cells*, vol. 187, pp. 140–153, Dec. 2018.
- [5] M. Bivour, S. Schröer, M. Hermle, and S. W. Glunz, "Silicon heterojunction rear emitter solar cells: Less restrictions on the optoelectrical properties of front side TCOs," *Sol. Energy Mater. Sol. Cells*, vol. 122, pp. 120–129, Mar. 2014.
- [6] T. Tohsophon, A. Dabirian, S. D. Wolf, M. Morales-Masis, and C. Ballif, "Environmental stability of high-mobility indium-oxide based transparent electrodes," *APL Mater.*, vol. 3, no. 11, p. 116105, Nov. 2015.
- [7] T. Minami, "Substitution of transparent conducting oxide thin films for indium tin oxide transparent electrode applications," *Thin Solid Films*, vol. 516, no. 7, pp. 1314–1321, Feb. 2008.
- [8] T. Koida, H. Fujiwara, and M. Kondo, "High-mobility hydrogen-doped transparent conductive oxide for a-Si:H/c-Si heterojunction solar cells," *Sol. Energy Mater. Sol. Cells*, vol. 93, no. 6–7, pp. 851–854, Jun. 2009.
- [9] Z. C. Holman *et al.*, "Current Losses at the Front of Silicon Heterojunction Solar Cells," *IEEE J. Photovolt.*, vol. 2, no. 1, pp. 7–15, Jan. 2012.
- [10] M. Balestrieri, D. Pysch, J.-P. Becker, M. Hermle, W. Warta, and S. W. Glunz, "Characterization and optimization of indium tin oxide films for heterojunction solar cells," *Sol. Energy Mater. Sol. Cells*, vol. 95, no. 8, pp. 2390–2399, Aug. 2011.
- [11] C. Zhou *et al.*, "SiOx(C)/SiNx dual-layer anti-reflectance film coating for improved cell efficiency," *Sol. Energy*, vol. 85, no. 11, pp. 3057–3063, Nov. 2011.
- [12] S. Y. Herasimenka, W. J. Dauksher, M. Boccard, and S. Bowden, "ITO/SiOx:H stacks for silicon heterojunction solar cells," *Sol. Energy Mater. Sol. Cells*, vol. 158, Part 1, pp. 98–101, Dec. 2016.
- [13] D. Zhang *et al.*, "Design and fabrication of a SiOx/ITO double-layer anti-reflective coating for heterojunction silicon solar cells," *Sol. Energy Mater. Sol. Cells*, vol. 117, pp. 132–138, Oktober 2013.
- [14] J. Geissbühler *et al.*, "Silicon Heterojunction Solar Cells With Copper-Plated Grid Electrodes: Status and Comparison With Silver Thick-Film Techniques," *IEEE J. Photovolt.*, vol. 4, no. 4, pp. 1055–1062, Jul. 2014.
- [15] R. Santbergen, A. H. M. Smets, and M. Zeman, "Optical model for multilayer structures with coherent, partly coherent and incoherent layers," *Opt. Express*, vol. 21, no. 102, pp. A262–A267, Mar. 2013.
- [16] A. Fell, "A Free and Fast Three-Dimensional/Two-Dimensional Solar Cell Simulator Featuring Conductive Boundary and Quasi-Neutrality Approximations," *IEEE Trans. Electron Devices*, vol. 60, no. 2, pp. 733–738, Feb. 2013.
- [17] A. Pflug, V. Sittinger, F. Ruske, B. Szyszka, and G. Dittmar, "Optical characterization of aluminum-doped zinc oxide films by advanced dispersion theories," *Thin Solid Films*, vol. 455–456, pp. 201–206, May 2004.
- [18] W. Kern, "The Evolution of Silicon Wafer Cleaning Technology," *J. Electrochem. Soc.*, vol. 137, no. 6, pp. 1887–1892, Jun. 1990.
- [19] A. B. Morales-Vilches *et al.*, "Nanocrystalline vs. amorphous n-type silicon front surface field layers in silicon heterojunction solar cells: Role of thickness and oxygen content.," *Proc EUPVSEC 2017*.
- [20] D. Pysch, A. Mette, and S. W. Glunz, "A review and comparison of different methods to determine the series resistance of solar cells," *Sol. Energy Mater. Sol. Cells*, vol. 91, no. 18, pp. 1698–1706, Nov. 2007.
- [21] A. Valla, P. Carroy, F. Ozanne, and D. Muñoz, "Understanding the role of mobility of ITO films for silicon heterojunction solar cell applications," *Sol. Energy Mater. Sol. Cells*, vol. 157, pp. 874–880, Dec. 2016.
- [22] K. Ellmer, F. Kudella, R. Mientus, R. Schieck, and S. Fiechter, "Influence of discharge parameters on the layer properties of reactive magnetron sputtered ZnO:Al films," *Thin Solid Films*, vol. 247, no. 1, pp. 15–23, Jul. 1994.
- [23] T. Koida, M. Kondo, K. Tsutsumi, A. Sakaguchi, M. Suzuki, and H. Fujiwara, "Hydrogen-doped In₂O₃ transparent conducting oxide films prepared by solid-phase crystallization method," *J. Appl. Phys.*, vol. 107, no. 3, p. 33514, Feb. 2010.
- [24] V. Srikant and D. R. Clarke, "Optical absorption edge of ZnO thin films: The effect of substrate," *J. Appl. Phys.*, vol. 81, no. 9, pp. 6357–6364, May 1997.
- [25] T. Koida, H. Fujiwara, and M. Kondo, "Reduction of Optical Loss in Hydrogenated Amorphous Silicon/Crystalline Silicon Heterojunction Solar Cells by High-Mobility Hydrogen-Doped In₂O₃ Transparent Conductive Oxide," *Appl. Phys. Express*, vol. 1, p. 41501, Mar. 2008.
- [26] K.-U. Ritzau, T. Behrendt, D. Palaferri, M. Bivour, and M. Hermle, "Hydrogen doping of Indium Tin Oxide due to thermal treatment of hetero-junction solar cells," *Thin Solid Films*, vol. 599, no. Supplement C, pp. 161–165, Jan. 2016.
- [27] D. B. M. Klaassen, "A unified mobility model for device simulation—I. Model equations and concentration dependence," *Solid-State Electron.*, vol. 35, no. 7, pp. 953–959, Jul. 1992.
- [28] A. Richter, S. W. Glunz, F. Werner, J. Schmidt, and A. Cuevas, "Improved quantitative description of Auger recombination in crystalline silicon," *Phys. Rev. B*, vol. 86, no. 16, p. 165202, Oct. 2012.
- [29] T. Trupke *et al.*, "Temperature dependence of the radiative recombination coefficient of intrinsic crystalline silicon," *J. Appl. Phys.*, vol. 94, no. 8, pp. 4930–4937, Sep. 2003.

- [30] H. H. Berger, "Models for contacts to planar devices," *Solid-State Electron.*, vol. 15, no. 2, pp. 145–158, Feb. 1972.
- [31] D. Adachi, "Effects of SiO_x barrier layer prepared by plasma-enhanced chemical vapor deposition on improvement of long-term reliability and production cost for Cu-plated amorphous Si/crystalline Si heterojunction solar cells."
- [32] A. B. Morales-Vilches *et al.*, "ITO-Free Silicon Heterojunction Solar Cells With ZnO:Al/SiO₂ Front Electrodes Reaching a Conversion Efficiency of 23%," *IEEE J. Photovolt.*, pp. 1–6, 2018.